# SEARCHING FOR MILLISECOND PULSARS IN GAMMA-RAY DATA USING THE FERMI LAT

A Thesis Submitted in Partial Satisfaction
Of the Requirements for the Degree of
Bachelor of Science in Astrophysics
at the
University of California, Santa Cruz

By
Nathan Ryan Frank
June 10, 2009

| Robert P. Johnson<br>Technical Advisor | David P. Belanger<br>Supervisor of Senior Theses |
|---|---|

David P. Belanger
Chair, Department of Physics

## Abstract

When professor Antony Hewish of Cambridge University set out with his graduate student Jocelyn Bell to study the effects of interplanetary scintillation in the latter part of 1967 he had no idea they would make one of the most important astronomical discoveries of their time. The association of their discrete radio signal with a Pulsar, then only a theorized entity, initiated an era of great interest in interstellar space. As further analysis was conducted a need for telescopes to monitor radiation at other energies became quite evident. Soon the first space based telescopes were launched in order to study high energy radiation, which is absorbed by the atmosphere. Although not the first probe into the gamma-ray sky, the Energetic Gamma Ray Experiment Telescope, or EGRET, aboard the Compton Gamma Ray Observatory (CGRO) lead to the discovery of a great many point sources of gamma-rays, many of which remained unidentified during its lifetime. Its successor, and in many ways superior, the Gamma Ray Large Area Space Telescope (GLAST), later renamed Fermi, was launched in June of 2008 and now allows for an even greater and more detailed exploration of the gamma-ray sky. One of the major science goals associated with the new telescope is the resolution of many unidentified point sources of gamma rays and the discovery of new pulsars. With more and better data, new search techniques have been implemented to find pulsars, most notably a time-differencing technique (Atwood et al. 2006, Ziegler et al. 2008). Using this technique and data from the Fermi telescope, blind searches have been performed to detect neutron star pulsations. Here I review the history and relevant science of pulsars as well as the telescopes used in their discovery. I also discuss the time-differencing technique and its use in the discovery of new pulsars. Finally, I provide analysis of the possibility for discovery of a new millisecond pulsar, a special class of rapidly rotating pulsars, in gamma-ray data alone.

## 1 – Pulsar Discovery

Although Jocelyn Bell's discovery of a periodic radio signal in August of 1967 lead to the first confirmed discovery of a pulsating source of radio (PSR), or pulsar, the seeds for such a discovery were laid by Walter Baade and Fritz Zwicky in 1934 (Baade and Zwicky 1934). They suggested the existence of a neutron star, a possible endpoint in stellar evolution:

> ...a supernova represents the transition of an ordinary star into a neutron star, consisting mainly of neutrons. Such a star may possess a very small radius and an extremely high density (Baade and Zwicky 1934)

It was also suggested by Pacini in 1967, prior to the discovery of the pulsar, that a highly magnetized, rapidly rotating neutron star may be the source of energy in the Crab Nebula (Pacini 1967). The 250-ft. radio telescope at Jodrell Bank in Manchester, U.K. had the ability to discover a pulsar about 10 years prior to the actual discovery; however, periodic fluctuations in the radio signal were either overlooked or not recognized as such. The implementation at Cambridge of a large receiving antenna with a longer wavelength (3.7 m) by Hewish allowed their telescope to be sensitive to weak discrete radio sources (Lyne and Graham-Smith 2005). The initial discovery of large signal fluctuations at similar times on successive days was dismissed as possible terrestrial interference until a recorder with a faster response time was used and, in November of 1967, a pulse with a period of 1.337 seconds was recorded (Lyne and Graham-Smith 2005).

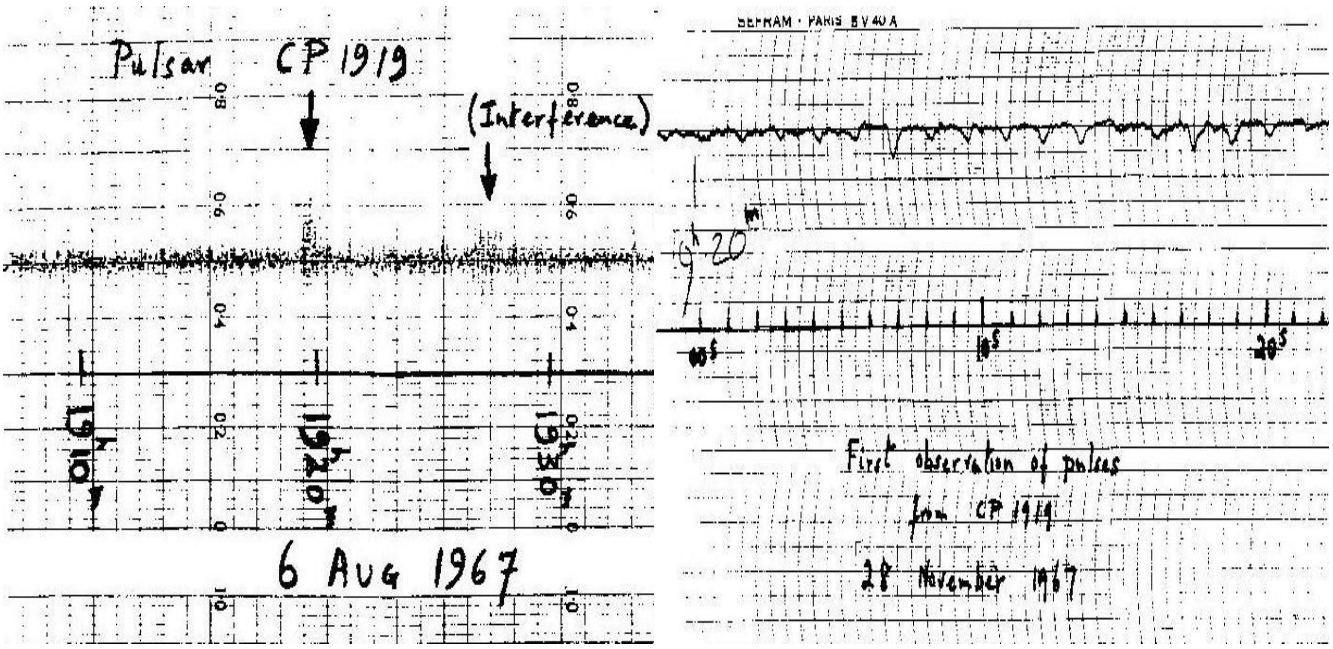


Figure 1: The left is the original recording of the first pulsar B1919+21 and the right is the fast recording. In the original you can see where the fluctuations were labeled as interference (Lyne and G-S 2005, taken from Hewish et al. 1968).

The discovery was announced in a Nature article of February 1968. The initial publication contained a great deal of analysis of the signal, first suggesting the source must lie outside the solar system due to Doppler effect observations on the pulsar periodicity (Lyne and Graham-Smith 2005). They reasoned that the short period of the signal implied its association with a compact object, either a white dwarf or neutron star. Initially, there were three proposed models for the source of such periodic signals: radial pulsations, orbital motion, and rotation. Radial pulsation and orbital motion were ruled out because of the short period, which was increasing with time. A rotating neutron star became the only possible candidate due to its stability at such a short period, low enough luminosity at closest pulsar distances, and small enough radius (Manchester and Taylor 1977). The first pulsar was named PSR B1919+21. The B stands for the location in 1950 coordinates while the numbers give the location in the sky. All pulsars published after 1993 are designated by a J, for J2000 coordinates, and have numbers referring to their right ascension and declination. Some older pulsars, therefore, are listed with two different names for the two systems (Lyne and Graham-Smith 2005).

## 2 – Pulsar Properties

In the first year following the discovery by Bell and Hewish a great deal of work was published concerning pulsars and when the dust settled it was generally accepted that pulsars are strongly magnetized and rapidly rotating neutron stars. Although theorized years before their discovery, much of what is now known about pulsars has been confirmed by observation and population statistics. In order to understand how pulsars came to be it is important to first break down the components which make them special, namely the formation of neutron stars, the role of their strong magnetic fields, and the nature of their evolution. I will also discuss the evolution of binary and millisecond pulsars, a class with somewhat distinct development and physical properties.

### 2.1 – Neutron Star Formation

Neutron stars are one of the possible endpoints in stellar evolution, along with black holes and white dwarfs. A star "dies" when it ceases to to generate energy through nuclear fusion in its core. More massive stars may be able to continue through the nuclear cycle to the burning of iron; however, others will be disrupted by hot flashes when the core begins to burn other elements such as oxygen (the "oxygen flash"). Without the thermal pressure due to nuclear energy generation the star cannot withstand the internal compression due to gravity and will collapse. This collapse occurs first in the inner core of the star, releasing enormous amounts of energy which blow way the outer layers of the star. Once the supernova explosion has occurred, gravity begins to pull the remaining stellar material in upon itself until another means of pressure support allows for an equilibrium state. Neutron stars are one example of this equilibrium, gaining the needed quantum mechanical neutron degeneracy pressure from the non-interaction of neutrons which, as fermions, are only allowed to have one particle occupying a given quantum mechanical state. Similarly, white dwarfs, another possible equilibrium

endpoint in stellar evolution, are supported by electron degeneracy pressure. Although it is impossible to know for sure what progenitor star formed each compact object, population statistics show that neutron stars likely evolved from 4-10 solar mass stars, often via a supernova explosion (Longair 1994). Neutron stars have an average mass of 1.4 solar masses ($2.8 * 10^{30}$ kg), although their mass can range between 0.2 and 2.0 solar mases. They have an average radius of 1.4 km, leading to a central density on the order of $10^{14}$-$10^{15}$ g/cm$^3$. Neutron stars consist of a neutron super-fluid interior housed within a crystalline solid crust and while its strong magnetic fields only minimally affect its interior makeup, playing a small role in the composition of the crystal structure of the crust, they are dominant in the region outside the star (Lyne and Graham-Smith 2005).

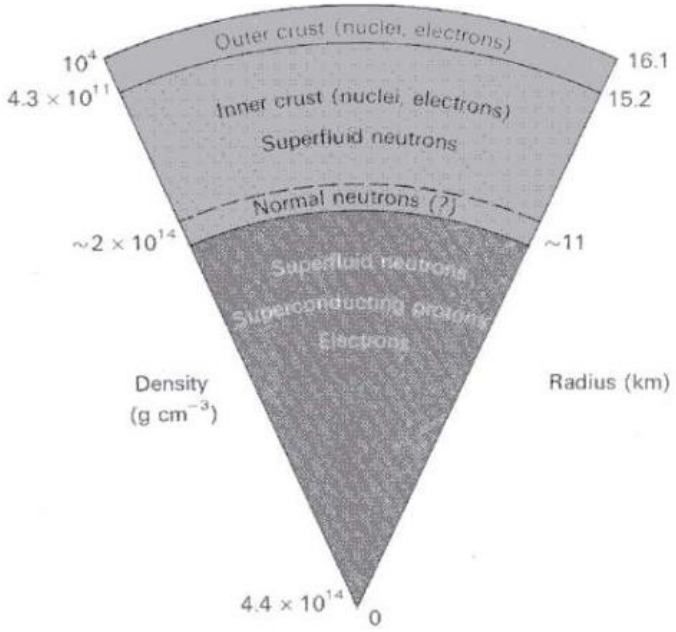


Figure 2: An example neutron star cross section (Manchester and Taylor 1977).

The association with supernovae has lead to realization of a number of important facts concerning pulsars. Supernova explosions explain pulsar's high transverse velocities, gaining kicks due to asymmetry in the explosion. These high drift velocities help explain pulsars being found away from

supernova remnants (SNRs) although likely being born in the same region. While most supernova remnants have a lifetime of about $10^5$ years, pulsars are known to "live" (be detectable) for about $10^7$ years (Longair 1994, Bhattacharya and Heuvel 1991). The Galactic pulsar birthrate has been estimated at about one per fifty years from statistics of supernovae. Furthermore, the predominant existence of pulsars as solitary objects while most other stars are members of binary systems is most likely due to disruption from the supernova explosion (Bhattacharya and Heuvel 1991).

## 2.2 – Pulsar Magnetic Fields

Pulsars have extremely strong magnetic fields associated with them which greatly affect the physical conditions far beyond the surface of the star. The magnetic field is also responsible for the loss of angular momentum due to magnetic dipole radiation. This loss of energy and angular momentum is what causes pulsar periods to lengthen over time. The magnetosphere is a region outside the surface of the pulsar but within the speed-of-light cylinder, a space with a radius such that a particle located at its edge and co-rotating with the pulsar would be traveling at the speed-of-light (Bhattacharya and Heuvel 1991). This co-rotation is due to the fact that the magnetosphere is coupled to the ions of the star's crust by the strong magnetic fields (Manchester and Taylor 1977). Magnetic field lines cannot close beyond the speed-of-light cylinder and thus remain as "open" field lines. It is along these open field lines that the plasma of charged particles is accelerated as a pulsar "wind." The region around the magnetic poles on the surface of the pulsar between closed field lines are known as the polar "caps," while the region further out, beyond the last closed magnetic field line is known as the outer magnetospheric "gap." It is from these regions that the beams of radiation originates, through an electron-positron cascade and secondary plasma of charged particles. Primary charged particles are accelerated along open field lines by strong electric fields induced by the rotation of the highly magnetized neutron star (Bhattacharya and Heuvel 1991). The inclination of the magnetic dipole with

respect to the rotation axis in pulsars gives rise to a lighthouse effect, lending to their pulsed nature. Furthermore, the two emission regions lead to multiple beam patterns for the different emission frequencies: a narrow radio beam and a wider gamma-ray beam.

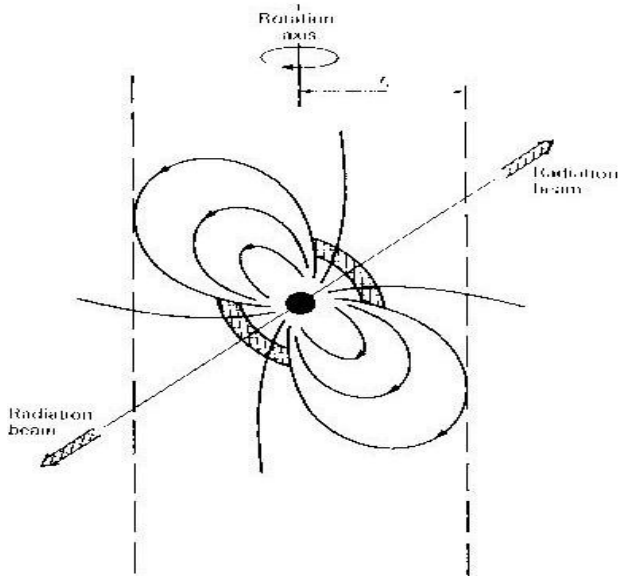


Figure 3: Pulsar schematic detailing essential features. The velocity of light cylinder is represented by the vertical dashed lines and the polar caps are the cross hatched regions (Lyne and Graham-Smith 2005).

Magnetic field strengths in young pulsars can reach $10^{12}$ Gauss, but among "normal" pulsars, population statistics tell us that those with longer periods (older) tend to have smaller average field strengths. An interesting value is the ratio of the gravitational to electrostatic forces on an electron near the surface of a pulsar. For the Crab Pulsar, the ratio $\frac{GMm}{r^2} / \frac{e\,\Omega\, rB}{c}$ is about $10^{-12}$ (21-22 Lyne and G-S). A measure of the strength of the magnetic field of a pulsar at its surface can be computed using its spin period and spin-down rate:

$$B_s = \left(\frac{3c^3 I}{8\pi^2 R^6} P\dot{P}\right)^{1/2},$$

where $I$ is the moment of inertia and $R$ the neutron star radius. These strong magnetic field strengths are generated in the collapse following supernova of a normal star with a field strength $B$ of about 100

Guass, the magnetic flux being conserved into compressing stellar material (Lyne and Graham-Smith 2005). Most calculations suggest that pulsar magnetic fields decay on a time scale of about $10^6$-$10^7$ years, based upon the time constant for field decay:

$$\tau_B = 4\sigma R^2/[\pi(m+1)c^2],$$

where σ is conductivity, *R* the stellar radius, and *m* an integer set to zero for a dipolar magnetic field (Manchester and Taylor 1977).

A decrease in magnetic field strength is generally thought to accompany the increasing period of a pulsar over time; however, the exact nature of the decay has been debated. A plot of field strength versus spin-down, or characteristic, age τ, defined as $\tau = 2\mathrm{P}/\dot{P}$ , shows a decrease in field strength with increasing τ. Another indicator of the age of a pulsar is called its kinetic age. This is defined as $t_k = z/\dot{z}$ where z is the distance the pulsar has migrated away from the galactic plane. Transverse velocity data indicate that pulsars have high velocities, with a population average of about 200 km/s. This allows them to travel great distances from the plane of our galaxy even though most are born very near to it. The magnetic field can be estimated from the spin period and spin-down rate suggesting the spin-down age τ is a good indicator of the true age if the magnetic field does not decay. However, when comparing the spin-down age τ to the kinetic age $t_k$, τ is on average two orders of magnitude larger. This means that "the spin-down age increases much faster than the true age, exactly as would be expected from a decay of the field strength" (Bhattacharya and Heuvel 1991). Further evidence suggesting the true age of pulsars is given by the characteristic age is found in observing characteristic ages for pulsars with associated supernova remnants. That of the Crab pulsar, 1,240 years, is close to the 955 years elapsed since its progenitor supernova; furthermore, the characteristic age of the Vela pulsar, $1.1 \cdot 10^4$ years, is in agreement with estimates of $1\text{-}3 \cdot 10^4$ years (Manchester and Taylor 2005).

In reality, a difference in kinetic versus spin-down age suggests a decline in the spin-down torque on the pulsar given by:

$$N = I\,\dot{\Omega} = \frac{2}{3c^3} B_s^{\,2} R^6 \Omega^3 \sin^2\alpha,$$

where Ω is the angular velocity and α the angle of inclination (Bhattacharya and Heuvel 1991). The similarly defined "radiation reaction torque" is given by:

$$N = -\frac{2(m\sin\alpha)^2}{3\mathrm{c}^3}\Omega^3,$$

where *m* is the magnetic dipole moment (Manchester and Taylor 2005). This has lead to theories which point to precession, or reduction of inclination α, of the magnetic dipole over time, leading to a decreased magnetic field (or magnetic moment) M due to alignment while the field strength B remains unchanged. Strong electric fields generated by the rapid rotation of the highly magnetized star give rise to a potential of $10^{14}$-$10^{15}$ volts. Before the realization that pulsars radiate a beam of radiation with two distinguishable components estimates of the dipole inclination angle α were impossible. This knowledge allows estimates of α to be made using the width of the core beam or the shape of the S-curve traced out by the rotating polarized beam (Bhattacharya and Heuvel 1991). However, no statistics showing a systematic trend in dipole inclination angle α have been found leading researchers to believe a decrease in magnetic field strength B is responsible for torque reduction (Bhattacharya and Heuvel 1991, Lyne and Graham-Smith 2005).

A good description of the life of a pulsar, and its magnetic field, can be found in analysis of a field-period (or B-P) diagram. Figure 6 below shows a *B*-*P* (field strength versus period) diagram and gives a good visual representation of the evolutionary life of most pulsars. They begin in the upper left corner and have strong magnetic fields and short periods and end lower and to the right with depleted

magnetic fields and extended periods. The stronger a pulsar's magnetic field at birth the faster its period will increase, especially initially. After a few million years of emission, the magnetic field begins to decay and the increase in period halts, since spin-down rate decreases with decreased magnetic field. Within about ten million years the polar cap voltage will decrease sufficiently that the pulsar will cease to radiate and become "invisible." This accounts for the lack of low B and long P pulsars, below the "death line" in the diagram. There is evidence to suggest that magnetic fields of pulsars do not decay completely but reach a minimum of no less that $10^8$ Gauss. Some pulsars are spun-up through accretion and are found in the lower left of the diagram. These are the binary (circled) and millisecond pulsars and will be discussed in more detail in later sections.

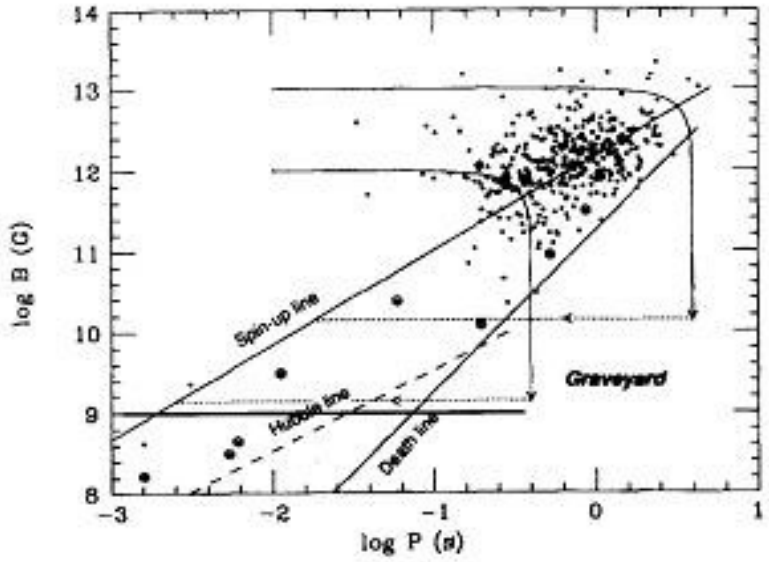


Figure 4: A *B-P* diagram showing the derived magnetic fields of 403 pulsars plotted against spin period (Bhattacharya and Heuvel 1991).

2.3 – Pulsar Emission

Pulsar emission emanates from two principal regions, core emission from the polar caps and cone emission from the outer gap. The development of the core beam of particles is dependent upon surface flow from the pulsar, either thermal or field emission, or as a result of a reverse flow of oppositely charged particles. Whatever the cause, a stream of particles with relativistic energies $\gamma$ of about $10^6$-$10^7$

is excited along magnetic field lines above the surface. This primary beam develops a broader cascade of charged particles through pair production. The electrons (or positrons) produced are restricted to following magnetic field lines, which are generally curved. As the particle is transversely accelerated it radiates gamma rays in a process known as curvature radiation. The cascade creates a secondary plasma of charged particles which has lower energy and higher density due to the emitted pairs. Since this takes place in a region of closed magnetic field lines, gamma rays produced continue to interact with the magnetic field, creating electron-positron pairs, and furthering the cascade. The resulting plasma of accelerated charged particles is responsible for the core radio emission from the polar cap region, explaining the much narrower radio beam produced by pulsars.

Radiation from the outer magnetospheric gap, the region bounded by the last closed field line and extending to the velocity of light cylinder, emanates in a similar cascade. The difference is that the electric field extends further, accelerating electrons and positrons to highly relativistic energies, without the damping effect of the plasma. As in the polar cap, curvature radiation is created by the charged particles moving along open field lines; however, the subsequent gamma rays produced may escape to be observed as high energy pulsar radiation or continue to aid in a particle cascade. The emission from the outer gap is responsible for a nearly constant beam pattern over more than ten decades of the Crab pulsar high-energy spectrum due to the geometrically restricted emitting region (Lyne and Graham-Smith 2005). Although the processes in these two regions are very similar, the details of their emission differ greatly. The figures below detail the emission regions and cascade processes.

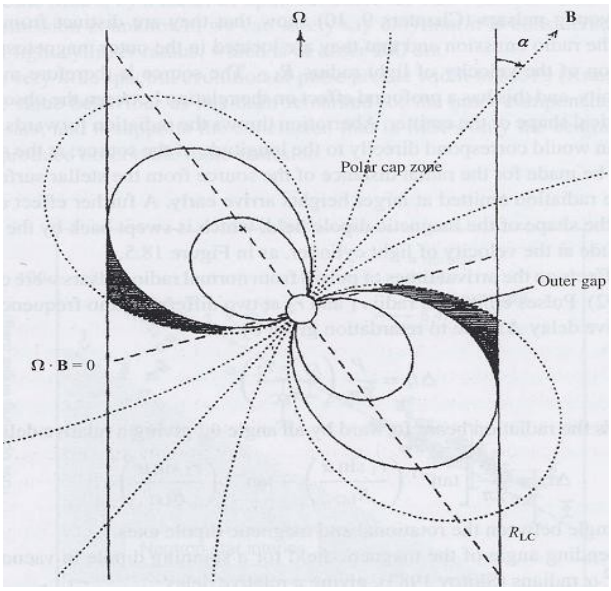


Figure 5: Schematic diagram of a pulsar detailing emission regions, notably the locations of the polar cap and outer magnetospheric gap (Chiang and Romani 1992).

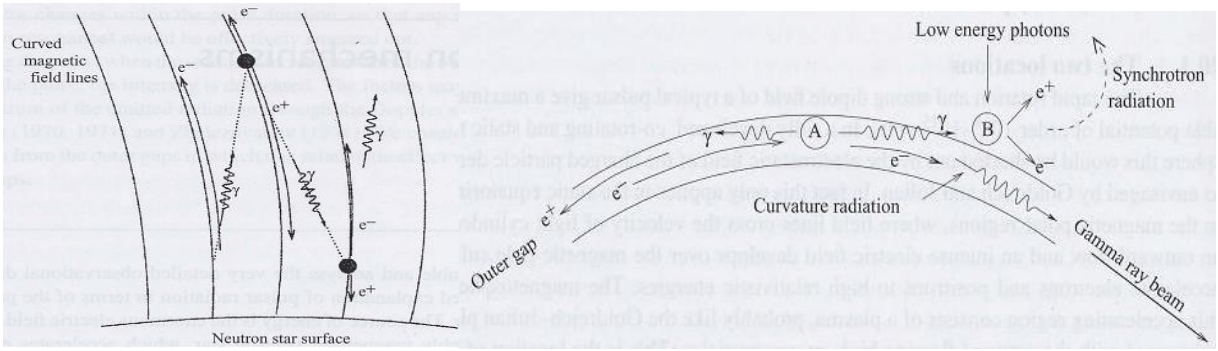


Figure 6: The left is an image detailing the cascade process in the polar cap region and the right is a similar representation of cascade process in the outer magnetospheric gap (Lyne and Graham-Smith 2005).

As previously noted, pulsars, although predominantly detected via radio emission, radiate energy through the full range of the electromagnetic spectrum. Optical pulses from the Crab Pulsar were discovered by Cocke, Disney, and Taylor on 16 January 1969 using a cathode-ray rube. Soon after, a stroboscopic photograph was taken at Lick Observatory using a new television technique. Also in 1969, two separate rocket flights successfully detected X-ray emission from the Crab Pulsar with radiated power more than 100 times greater than in the visible region (Lyne and Graham-Smith 2005). These discoveries provided many answers concerning details of pulsar emission and laid the

groundwork for further research into high energies as well as into binary and millisecond pulsars, common emitters of high energy radiation.

High energy emission is most commonly associated with younger pulsars, although older millisecond pulsars are capable of high energy emission as well. The key source of energy fueling the emission is the rate of loss of rotational energy, given by:

$$\dot{E} = -I\,\Omega\,\dot{\Omega} = -4\pi^2 I\,\nu\,\dot{\nu} = 4\pi^2 I\,\dot{P}/P^3.$$

Clearly, the high energy output of young and millisecond pulsars is due to their very low spin periods and, in the case of young pulsars, large period derivatives. Since the inertia is mostly independent of the neutron star model adopted, and varies little with mass, the period and period derivative are important in determining energy output. For the Crab pulsar the energy loss rate is $\dot{E} = 4.5 \cdot 10^{38}$ erg $s^{-1}$. Much, at least $1.5 \cdot 10^{38}$ erg $s^{-1}$, must be absorbed in the surrounding Crab Nebula in order to account for observed radiation. Non-thermal X-rays, generated by synchrotron (or magnetic bremsstrahlung) radiation, where charged particles are accelerated to relativistic energies in a magnetic field, are seen as pulsed emission (Lyne and Graham-Smith 2005). Both the X-ray and gamma-ray emission are emitted from the outer magnetospheric gap as a wide cone of emission. The highest energy gamma-rays, of up to TeV energies, are emitted furthest out in the outer gap, where the magnetic field is weakest and pair production is less limited (Lyne and Graham-Smith 2005).

## 3 – Binary and Millisecond Pulsars

X-ray emission from X-ray binary pulsars is usually generated during the accretion of mass from one star onto another. Before the class of X-ray binaries and the nature of their emission can be discussed, however, it is important to understand how they are formed and what separates them from “normal”

pulsars. From a statistical standpoint, there are many factors which differentiate the population of binary and millisecond pulsars, related by their method of formation, from the majority of the population of pulsars. Both binary and millisecond pulsars tend to have much weaker magnetic fields and much shorter periods than the bulk of pulsars. Furthermore, about half of millisecond pulsars lie in binary systems, while about 92% of pulsars in general are solitary (Manchester et al. 2005). Finally, as will be discussed, the formation of millisecond pulsars, both solitary and binary, is closely related to the evolution of binary pulsar systems and share important traits with a particular class of X-ray binaries. Although binary and millisecond pulsars represent a minority of the pulsar population, their study has done a great deal to further knowledge of neutron stars and their magnetic fields (Bhattacharya and Heuvel 1991).

Since the discovery of discrete X-ray sources many have displayed periodic variations in both optical and X-ray emission suggesting they are members of close binary systems. Optical observations also allow for a more complete analysis of the system to be made, including the masses of the separate components. A spectroscopic Doppler shift observation of the radial velocity of the visible star also allows measurements of the orbital periods of binary systems to be made and are often on the order of a few days, suggesting a system close enough for mass transfer. When the velocity curve of the visible star is resolvable it can be combined, along with Newtonian mechanics for elliptical orbits, to yield the mass function:

$$f(m_p, m_c, i) = \frac{4\pi^2}{G}\frac{a^3 \sin^3 i}{P_b^{\,2}} = \frac{m_c^{\,3}\sin^3 i}{(m_p + m_c)^2}$$

where $m_p$ is the primary star (pulsar) mass, $m_c$ the companion mass, $i$ the inclination of the orbit with respect to the plane of the sky, $P_b$ the period of the binary orbit, and $G$ the gravitational constant. In most cases, when velocity curves for the sources are obtained, separate mass can be determined for

each member of the system and are generally about 2-30 solar masses for the visible companion and 1-3 solar masses for the primary X-ray source, determined to be a pulsar by the same logic used for the radio emitters (Manchester and Taylor 1977, Lyne and Graham-Smith 2005).

3.1 – Accretion in X-ray Binaries

Data indicate the majority of X-rays from discrete sources are due to accretion of matter from the massive companion star onto the compact primary. This is thought to be the principal process producing X-ray emission in X-ray binaries; however, solitary X-ray emitters have been found and their emission is likely due to rotation of the neutron star as in most pulsar emission. Still, other X-ray emitters have been found with long period emission (6-12 s), extremely strong magnetic fields ($10^{14}$-$10^{15}$ Gauss), and high luminosity. However, their spin-down energies $I\omega\dot{\omega}$ are far too low to account for their luminosities and the nature of their emission is unknown, lending to the name anomalous X-ray pulsar (AXP). Similar to AXPs is a class of radio pulsars which also have very strong magnetic fields, together they form a class known as 'magnetars', with the source of the X-ray energy being stored in the magnetic field in the interior of the neutron star. Isolated X-ray emitters have also been detected through soft emission of thermal X-rays from the surface of the neutron star, the source of which is most likely energy stored in the gravitational collapse (Manchester and Taylor 1977, Lyne and Graham-Smith 2005).

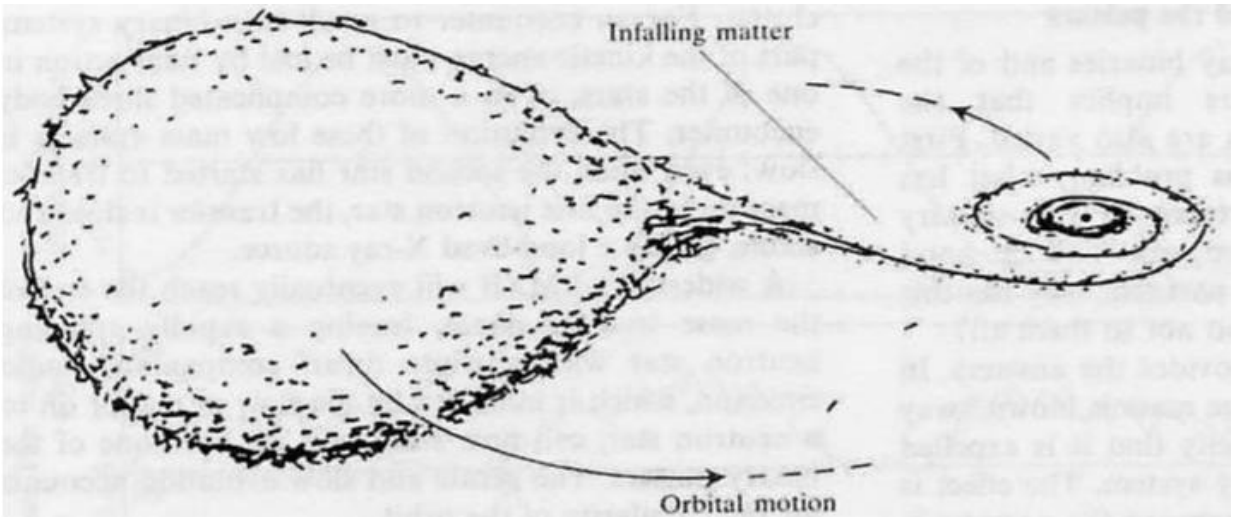


Figure 7: Matter streams onto the compact neutron star from the massive companion, transferring angular momentum in the process (Francis Graham-Smith 1992).

The primary emission mechanism of interest is that due to accretion in a binary star system, shown above. The X-ray luminosity of the pulsar is approximately equal to the rate of potential energy loss of the accreting material:

$$L_x \approx \frac{G M \dot{M}}{R},$$

where $M$ and $R$ are the mass of the compact star and $\dot{M}$ is the accretion rate. The maximum X-ray luminosity is known as the Eddington luminosity $L_{Edd}$, and is derived from an equilibrium between gravitational forces and the radiation pressure, using the relation:

$$\frac{GM}{r^2} = \frac{L \sigma_{el}}{4 \pi r^2 m_p c},$$

and equal to:

$$L_{Edd} = \frac{4 \pi G M m_p c}{\sigma_{el}},$$

where $r$ is the distance to the star, $M$ the neutron star mass in solar masses, $G$ the gravitational constant, $c$ the speed of light, $m_p$ is the proton mass, and $\sigma_{el}$ is the Thompson cross section of the electron (Bhattacharya and Heuvel 1991). If the radiation pressure is less than $L_{Edd}$ then the outward pressure on

the electrons of the accreting plasma will be less than the inward gravitational pull on the protons of the plasma, allowing accretion. Using $L_{Edd} = 1.3 \times 10^{38} M/M_\odot$ erg $s^{-1}$ ($M_\odot$ is the mass of the Sun) sets the maximum expected X-ray luminosity at $2 \times 10^{38}$ erg $s^{-1}$, agreeing well with maximum observed luminosities of $\sim 10^{38}$ erg $s^{-1}$. This value leads to accretion rates in the range $10^{-10}$ to $10^{-8}$ $M_\odot$ per year (Lyne and Graham-Smith 2005, Manchester and Taylor 1977). Greater rates of accretion, up to $10^{-6}$ $M_\odot$ per year are theoretically possible, however, no change in luminosity is observed as any rise in luminosity would prevent accretion from continuing. Accreted material is transferred from the companion star due to either: (a) expansion of the star off the main sequence, causing it to fill its Roche lobe (critical potential lobe) and transfer mass in a disk through the Lagrangian point L1; or (b) a stellar wind.

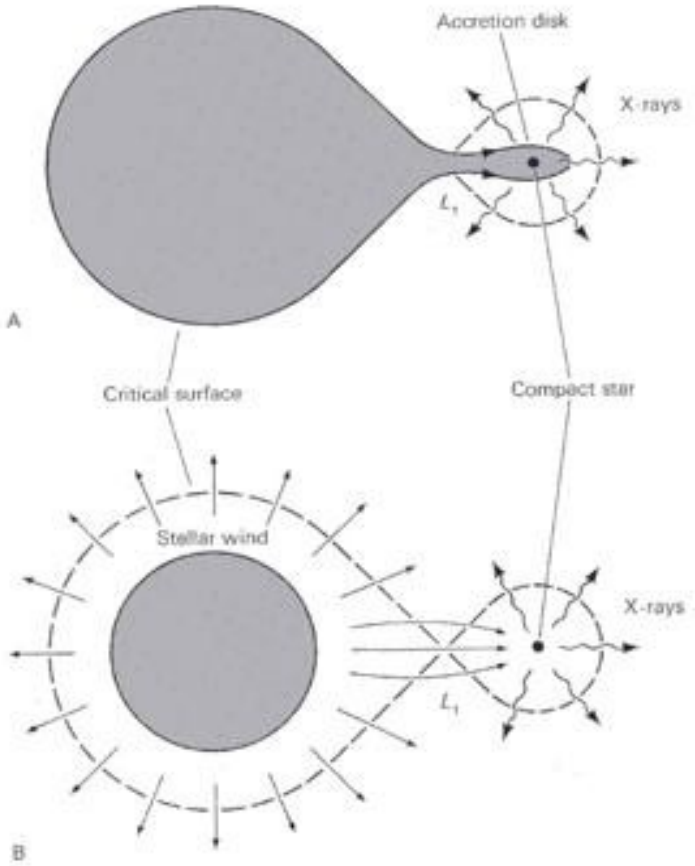


Figure 8: Two manners of accretion: a) due to Roche love overflow and b) due to a stellar wind (Manchester and Taylor 1977).

The two classes of strong galactic X-ray sources.

| Class I | Class II |
|---|---|
| – Relatively hard X-ray spectra: $kT \gtrsim 15$ keV | – Softer X-ray spectra: $kT \lesssim 10$ keV |
| – Type of time variability: regular X-ray pulsations; no X-ray bursts | – Type of time variability: often X-ray bursts; only in three cases regular X-ray pulsations |
| – Concentrated in space towards the galactic plane: young stellar population, age $< 10^7$ yr | – Concentrated in space toward the galactic center; fairly wide spread around the galactic plane: old stellar population, age $(5–15) \times 10^9$ yr |
| – Optical counterparts massive and luminous early-type stars, spectrum O and early B; $L_{opt}/L_X > 1$ | – Faint blue optical counterparts; $L_{opt}/L_X < 0.1$ |

Figure 9: A table listing the basic properties of HMXBs (Class I) and LMXBs (Class II) (Bhattacharya and Heuvel 1991).

3.2 – Low and High Mass X-ray Binaries

The first process discussed above is that associated with low-mass X-ray binaries (LMXBs), where the companion star is a (less luminous) main sequence star, several identified as K-type stars. LMXBs generally have companion star masses of around, or less than, a solar mass, usually being less than the primary neutron star. LMXBs are also much rarer, even though they involve a more common star type which evolves slowly (Francis Graham-Smith 1992). The second process is associated with high-mass X-ray binaries (HMXBs), in which the companion star is a supergiant or Be type star, whose naturally high luminosity tends to drive the stellar wind (Lyne and Graham-Smith 2005, Manchester and Taylor 1977). HMXBs are capable of transferring mass via either mechanism; however, the low mass companion in LMXBs does not usually have sufficiently high luminosity to propel a stellar wind. Furthermore, HMXBs with B-emission-type companions ("Be" systems) differ in their properties and mass transfer mechanism. In standard HMXB systems companion stars tend to be evolved giant or supergiant stars with radii 10-20 $R_\odot$ , optical luminosity greater than $10^5$ $L_\odot$ and initial masses of more than 20 $M_\odot$ (where the subscript $\odot$ refers to units of the Sun). In contrast, Be companion stars have smaller radii (< 5-10 $R_\odot$), luminosities ($< 3 \cdot 10^4$ $L_\odot$), and masses (8 – 20 $M_\odot$). Also, Be stars reside

deep inside their Roche lobes, making them incapable of mass transfer through Roche-lobe overflow (Bhattacharya and Heuvel 1991). The Be stars instead seem to transfer mass by a stellar wind or mass ejection from their equatorial region. The lack of Roche-lobe overflow is further evidenced by the transient nature of their emission, sometimes being unobservable for long periods of time and then suddenly turning on as strong X-ray sources for a period of time (Bhattacharya and Heuvel 1991). In addition to having high and low mass partners, binary pulsars can be involved in both close and wide systems. This attribute can greatly affect the evolution of the system, allowing dramatic interaction between the partners in which the neutron star can be absorbed by its companion in close binaries or the system disrupted in wide binaries (Francis Graham-Smith 1992).

Often, a neutron star born in a binary system will be undetectable as a pulsar because its signal will be disrupted by the stellar wind of the companion star, assuming the companion is not ejected by a supernova explosion. Following standard stellar evolution, the neutron star will generally cease emission before the companion expands and begins to transfer its mass. If the magnetic field of the neutron star is sufficiently strong enough it will be able to channel the inflowing material to its magnetic poles, lending to pulsed emission from the two hot X-ray emitting gas columns (Bhattacharya and Heuvel 1991).

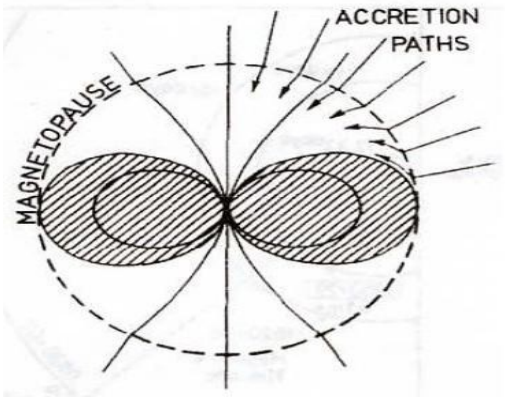


Figure 10: Visual representation of the accretion path of matter onto a neutron star (Bhattacharya and Heuvel 1991).

3.3 – Spin-Up Mechanism and Millisecond Pulsars

The transfer of mass onto the neutron star will impart angular momentum from the binary orbit, the value of which depends highly on the rate of mass transfer. This process leads to a "spin-up" of the neutron star, revitalizing its pulsed emission and returning it from the grave, so to speak (Lyne and G-S, Bhattacharya and Heuvel 1991). This spin-up process will end when the neutron star reaches an equilibrium spin period $P_{eq}$ which, for a particular accretion rate, is given by:

$$P_{eq} = 2.4\text{ms} \cdot \frac{B_9^{6/7}}{M^{5/7}(\dot{M}/\dot{M}_{Edd})^{3/7}} R_6^{16/7},$$

where $B_9$, $M$ and $R_6$ are the surface dipole magnetic strength in units of $10^9$ Gauss, the neutron star mass, and neutron star radius in units of $10^6$ cm, respectively (Bhattacharya and Heuvel 1991).
is the maximum possible accretion rate at which the luminosity due to accretion equals that of the Eddington luminosity, above which the accretion would be limited by radiation pressure, as previously discussed. For a standard neutron star of 10 km, $\dot{M}_{Edd} = 1.5 \cdot 10^{-8}\ M_\odot\ yr^{-1}$. As matter flows onto the neutron star it reaches an equilibrium barrier known as the Alfvén radius, which is defined as the distance where the energy density of the magnetic field equals the kinetic energy density of the inflowing plasma. Inside $R_A$ the inflowing matter from the disk will be coupled to the magnetic field lines of the neutron star and the magnetic field dominates its motion, causing it to co-rotate with the star. Outside this distance, the matter will move freely in Keplerian orbits. Matter enters the magnetosphere at a radius equal to $R_A$ along open field lines. The value for $P_{eq}$ is defined as the spin period at which the angular velocity of the neutron star is equal to the Keplerian angular velocity of the material in the accretion disk (Bhattacharya and Heuvel 1991). For periods greater than $P_{eq}$, accretion is possible and leads to the aforementioned spin-up. However, for periods below $P_{eq}$, built up matter at the Alfvén radius will exert braking torques on the magnetosphere, causing spin-down.

This process of recycling old pulsars through a spin-up mechanism is thought to explain the extremely low periods of millisecond pulsars, defined to have spin periods of less than 10 milliseconds, as well as the age of some binary and millisecond pulsars, up to $10^{10}$ years old. Using average values of 1.4 solar masses and a radius of 10 km for the neutron star, the equation for equilibrium period can be simplified to depend on magnetic field strength only: $P_{eq} = 1.89 \text{ ms} \cdot B_9^{6/7}$. This is what is known as the "spin-up line" in Figure 6 above. Recycled pulsars are expected to lie between the death line and spin-up line, as is evidenced by the existence of binary and millisecond pulsars in that region of the graph (Bhattacharya and Heuvel 1991). Of the millisecond pulsars in the galactic plane, 8 out of 13 are solitary due to either wide binary systems disrupting, their companions being dissolved by pulsar wind, or evaporation of large disks in spun-up pulsars, making them appear single (Bhattacharya and Heuvel 1991). Often, the end product of HMXBs is a system of a recycled pulsar and a compact object, often another neutron star. In one such case, a double pulsar binary system resulted. Close LMXBs most likely become solitary emitters by evaporating their companions, as is the case with most millisecond pulsars. However, the majority of recycled pulsars seem to be found orbiting a white dwarf companion as a result of LMXBs (Possenti and Burgay 2008). Pulsars from binaries can also become isolated by secondary supernova explosions of their companions (Bhattacharya and Heuvel 1991).

Today, the Australia Telescope National Facility reports that ~85% of pulsars have pulse periods between 100 ms and a few seconds (Manchester 2005, ATNF 2009). For many years after the discovery of the Crab Pulsar it had the shortest known period at 33 ms. With a large increase in computer capability since the discovery of the first pulsars the ability to detect those with periods shorter than 10 ms, previously not searched for due to the difficulty, has become possible and many have been found. These millisecond pulsars are unlike their younger, short period cousins, having been rescued from the graveyard and allowed to live at least 100 million years, better than 10 times

longer than most pulsars (Francis Graham-Smith 1992). Their peculiar arrangement of long life but short period is one of a number of factors that has set them apart from the normal pulsar population. Millisecond pulsars also tend to have much weaker magnetic field strengths, both as a result of decay due to their old age and field weakening during accretion. Furthermore, in order to reach a period of less than 10 ms, the magnetic field strength B at the time of spin-up should be less than $6 \cdot 10^9$ Gauss (Heuvel 1987). Although closely linked to binary systems, millisecond pulsars can be found alone, either due to a supernova of the companion disrupting the binary system or coalescence with the companion (Heuvel 1987). Others have suggested that asymmetric accretion of a large amount of energy and momentum could disrupt the system (Backer et al). Millisecond pulsars also have distinctly slow transverse velocities (~ 100 km/s) and tend to lie farther from the Galactic plane; however, this latter fact could be due to the difficulty of detecting MSPs along the galactic plane, especially at large distances (Possenti and Burgay 2008).

## 4 – Search Methods

The methods and technologies used in the discovery and observation of pulsars have changed significantly in the more than forty years since they were first discovered. Amazingly, however, the stability of pulsar emission, to better than one part in $10^{12}$ over many years, has continually made them one of the most widely studied astronomical objects (Manchester and Taylor 1977). Today, telescopes cover the full range of energies, gathering data across miles of land at locations around the globe or from space while orbiting the Earth. Furthermore, our ability to analyze the data has changed considerably from the days of pen-chart recordings to the current analysis performed with some of the world's fastest computers. Over the years many surveys have been conducted to gather data from large portions of the sky and identification of especially interesting discrete sources has lead to searches

which concentrate largely on specific targets. The bulk of of known pulsars were discovered via large radio surveys; however, much of today's work focuses on specific objects in order to analyze, among other things, the nature of their high-energy emission, gravitational field theories, and specific clues into their formation and evolution. With the discovery of binary and millisecond pulsars, as well as gamma-ray emitters, new and inventive analysis methods have been necessary to further knowledge of their less than basic properties.

4.1 – Telescopes

The first pulsar discovery was made using a radio telescope consisting of a rectangular array of 2,048 full-wave dipoles running at 81.5 MHz and spanning over almost 5 acres. Subsequent searches and surveys were performed at many of the larger radio telescopes of the world, including the Mills Cross at Molonglo, Australia, the 92 m transit paraboloid at Green Bank, West Virginia, and the 305 m spherical reflector at Arecibo, Puerto Rico. The immediate discovery of many more pulsars upon announcement of the first was a direct result of the ability of the varied telescopes to cover a large portion of the sky with highly sensitive, fast recording machines (Manchester and Taylor 1977). In fact, with so many radio telescopes constantly monitoring such a large fraction of the sky it is curious that pulsars were not discovered sooner. As previously mentioned, analysis of older recordings made clear that pulsars had gone unnoticed in collected data for some time. However, while the existing telescopes were fully capable of detecting pulsars, their implementation and analysis needed to change in order to see the majority of them. Only the first few pulsars were discovered (at Cambridge, Jodrell Bank, and Molonglo) as a result of individual pulse recordings. Future searches and surveys implemented a longer integration time and superposed many pulses at a particular periodicity, resulting in increased sensitivity. This method, although sound in theory, required the use of Fourier-like computational techniques in order to search over the range of possible unknown parameters, such as

period, pulse width, and dispersion measure. A table listing the main surveys viewing a significant portion of the sky which, in total, account for approximately three-quarters of known pulsars is shown below (Lyne and Graham-Smith 2005).

| Observatory | $\nu_{MHz}$ | $\Delta\nu_{MHz}$ | $T_{samp}$ (ms) | $S_{min}$ (mJy) | Sky coverage | Pulsars found | Ref.[a] |
|---|---|---|---|---|---|---|---|
| Molonglo | 408 | 4 | — | — | | 31 | 1,2 |
| Jodrell | 408 | 4 | 40 | 10 | $0° < l < 40°$ $\lvert b\rvert < 10°$ | 31 | 3,4 |
| Arecibo | 430 | 8 | 5.6 | | $35° < l < 75°$ $170° < l < 75°$ $\lvert b\rvert < 4°$ | 31 | 5,6 |
| Molonglo | 408 | 4 | 10 | | $\delta < +20°$ | 155 | 7 |
| Greenbank | 408 | 16 | 16 | | $\delta > 20°$ | 23 | 8 |
| Greenbank | 390 | 16 | 16 | 2 | $\delta > -18°$ | 34 | 9,10 |
| Greenbank | 390 | 8 | 2 | 3 | 3725 sq. deg | 20 | 11 |
| Jodrell | 1400 | 40 | 2 | 1 | $-5° < l < 95°$ $\lvert b\rvert < 1°$ $95° < l < 105°$ $\lvert b\rvert < 0°.6$ | 40 | 12 |
| Parkes | 1500 | 80/320 | 0.3/1.2 | 2.5/1.0 | $270° < l < 20°$ | 46 | 13 |
| Arecibo | 430 | 10 | 0.25 | 0.2 | 2128 sq. deg | 19 | 14 |
| Parkes | 436 | 32 | 0.3 | 3 | entire S. sky | 101 | 15 |
| Arecibo | 430 | 8 | 0.25 | 0.5 | 680 sq. deg | 12 | 16 |
| Arecibo | 430 | 8 | 0.2/0.3 | 0.7 | 960 sq. deg | 12 | 17 |
| Parkes | 1374 | 96 × 3 | 0.125 | 0.5 | $5° < \lvert b\rvert < 15°$ $-100° < l < 50°$ | 69 | 18 |
| Parkes PMBS | 1374 | 96 × 3 | 0.25 | 0.17 | $\lvert b\rvert < 5°$ $260° < l < 50°$ | 700 | 19, 20, 21 |

[a] 1. Large *et al.* 1968; 2. Vaughan *et al.* 1969; 3. Davies *et al.* 1970; 4. Davies & Large 1970; 5. Hulse & Taylor 1974; 6. Hulse & Taylor 1975; 7. Manchester *et al.* 1978a; 8. Damashek *et al.* 1982; 9. Stokes *et al.* 1985; 10. Dewey *et al.* 1985; 11. Stokes *et al.* 1986; 12. Clifton *et al.* 1992; 13. Johnston *et al.* 1992; 14. Foster *et al.* 1995; 15. Manchester *et al.* 1996; 16. Camilo *et al.* 1996b; 17. Ray *et al.* 1996; 18. Edwards *et al.* 2001; 19. Manchester *et al.* 2001; 20. Morris *et al.* 2002; 21. Kramer *et al.* 2003a

Figure 11: Table showing general aspects of major searches and surveys (Lyne and Graham-Smith 2005).

While the majority of known pulsars were found as a result of large scale surveys with radio telescopes, observations of their emission at X-ray and gamma-ray energies have significantly added to our understanding of them. Furthermore, X-ray and gamma-ray emission, produced at the outer gap of the pulsar, emanates in a wider cone than the radio emission, often allowing for a higher likelihood that its beam will pass over Earth. Although X-ray data collected by balloon and rocket flights of the 1960's were not initially understood, analysis lead to the notion of X-ray binaries. The UHURU satellite survey furthered our understanding of X-ray sources, including the possibility for mass transfer.

Orbiting telescopes have broadened the field of X-ray astronomy, beginning with the first all-sky survey by ROSAT, with an angular resolution of 1.2 arcminutes. This resolution was improved to 1 arcsecond by the Chandra and XMM-Newton X-ray telescopes. These orbiting telescopes detected X-ray pulsations from many isolated radio pulsars, suggesting energy for the emission is provided by the rotation of the neutron star rather than mass transfer in a binary system. Further advances in the field of X-ray astronomy were achieved by the Rossi X-ray Timing Explorer (RXTE), the first to achieve accurate pulse timing and with adequate time resolution to detect X-ray pulsations from millisecond pulsars (Lyne and Graham-Smith 2005).

Gamma-ray telescopes have since furthered our understanding of high-energy pulsar emission by greatly extending the available spectrum. Although the sensitivity achieved by these telescopes is generally several orders of magnitude less than for radio or X-ray detectors, the ability to analyze higher energy emission has greatly furthered our understanding of pulsar physics. A basic time line of gamma-ray telescopes important to pulsar astronomy is listed in the figure below, and the properties of some are detailed as follows. Gamma-ray maps of the galaxy were first developed by the SAS-2 and COS-B satellites of the 1970's, which also showed the first gamma-ray emission from the Crab and Vela Pulsars as well as initial observations of the Geminga source. The Compton Gamma-Ray Observatory (CGRO) was the first major gamma-ray observatory, providing many significant breakthroughs in the area of high-energy pulsar studies (153 Lyne and Graham-Smith 2005). Operating during much of the 1990's, CGRO covered a large energy range (30 keV-30GeV) and carried with it four separate instruments; the Burst and Transient Source Experiment (BATSE), the Oriented Scintillation Spectrometer Experiment (OSSE), the Compton Telescope (COMPTEL), and the Energetic Gamma Ray Experiment Telescope (EGRET) (Goddard Space Flight Center 2009). Due to the high energies of the photons being detected new methods must be used to observe their sources,

including: absorption of the photons using Sodium-Iodide scintillation crystal detectors, collimation and background rejection, and conversion of the photon into an electron-positron pair in a spark chamber. This combination of detectors allowed monitoring of the whole sky, albeit with a relatively poor angular resolution of 3º, or small points of ~ .6 steradian with a resolution of several arcminutes (Goddard Space Flight Center 2009). The third EGRET catalog listed 271 point sources of gamma rays with energies over 100 MeV of which many were left unidentified (Hartman et al). The European Space Agency's successor to COS-B and CGRO, the International Gamma-Ray Astrophysics Laboratory (INTEGRAL), uses a spectrometer and CdTe pixel imaging array to make a complete map of the gamma-ray sky with improved sensitivity and a spatial resolution of 12 arcminutes (European Space Agency 2009, Lyne and Graham-Smith 2005). The recently launched GLAST telescope has provided a remarkable improvement in sensitivity and field of view and has already proved important in the study of gamma-ray pulsars.

## 4.2 – The Fermi Satellite

The Gamma-Ray Large Area Space Telescope (GLAST), now known as the Fermi Gamma-Ray Space Telescope, was launched by NASA on June 11, 2008 aboard a Delta II Heavy rocket. The principle instrument of interest aboard Fermi is the Large Area Telescope (LAT), which is a high-energy gamma-ray, imaging telescope with a wide field-of-view. The telescope collects incident gamma-rays and measures their directions, energies, and arrival times, while also rejecting background cosmic rays. It covers the energy range from 20 MeV to 300 GeV with a 2.4 steradian field-of-view, covering nearly 20% of the sky at a given time. The LAT is a pair-conversion telescope, utilizing a precision converter-tracker and calorimeter in a 4 x 4 array of 16 planes of high-Z material covered by an anticoincidence detector (ACD) to monitor the conversion of a gamma-ray into an electron-positron pair (Atwood et al. 2009). Prompt signals from the tracker, calorimeter, and anticoincidence detector are sent to a

programmable trigger and data acquisition system to make up the trigger system. A particular feature of this trigger design is its self-triggering capability, made possible by the choice of silicon-strip detectors. The combination of position sensitive detectors interwoven into the converter planes can record the track of charge particles and thus reconstruct the directions of incident gamma-rays. The calorimeter serves the main purposes of measuring the energy produced by the particle shower resulting from the electron-positron pair and imaging the shower development. It has 96 CsI crystals for each module arranged to allow spatial imaging of the particle shower and aid in background rejection. The ACD is required to provide at least 0.9997 efficiency for detection of charged particles entering the LAT field-of-view, allowing for sufficient background rejection and meeting the 0.99999 efficiency requirement when combined with the other subsystems. The LAT has a number of science objectives, but those most interesting in the view of pulsar astronomy include: revolve the gamma-ray sky, determine the nature of unidentified sources, and understand the methods of particle acceleration in celestial sources (Atwood et al. 2009). With increased sensitivity over a wide field-of-view and energy range, the LAT aboard the Fermi satellite is expected to find many new gamma-ray pulsars.

## 4.3 – Data Analysis

Searching the radio telescope output for a periodic pulse signal can be done in two different ways. The first is to analyze the data itself for a series of regularly spaced pulses, as done for the initial pulsar discoveries. The other method, more commonly used today because it is less taxing on computers, is to analyze the Fourier transform of the data to find the spectrum of the pulses. The first, or periodogram, method divides the stream of $N$ regularly spaced pulses by a set of $N$ possible periods, creating many profiles which then must be scanned for pulses of various widths and phases. The sensitivity of the search depends on the pulse width such that a narrow pulse of width $W$ has an increased signal-to-noise ratio by a factor of $(P/2W)^{1/2}$ over a sinusoidal pulse with the same average flux (Lyne and Graham-

Smith 2005). The Fourier method analyzes the Fourier transform of the time data for fundamental frequency signals, as well as any associated harmonics. In a nearly sinusoidal pulse profile, there will be a large fundamental signal with small harmonics, while for a narrower pulse of width *W* there will be about *P*/2*W* harmonics with comparable amplitude to the fundamental (Lyne and Graham-Smith 2005). The figure below depicts the relationship between the time and frequency for Fourier transform of a pulse train with period *P* and pulse width *W*.

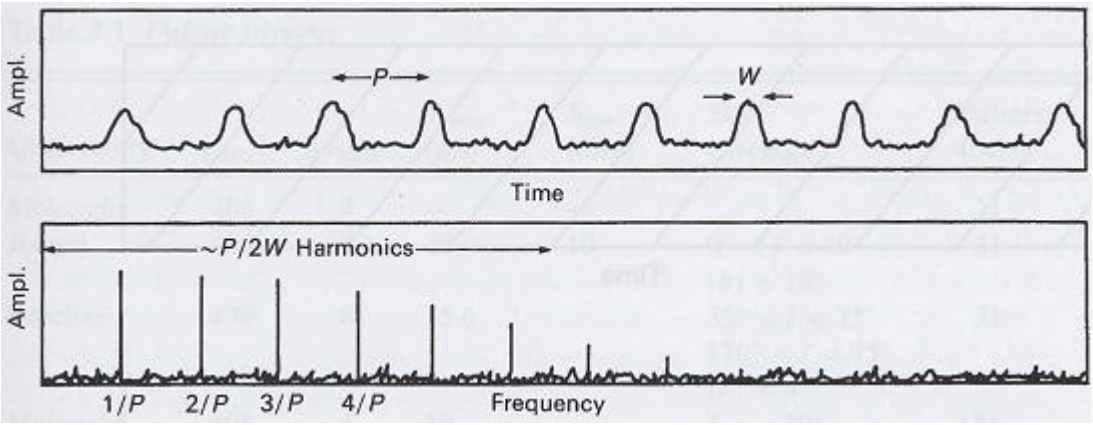


Figure 12: Correlation of frequency to time in a Fourier transform (Lyne and Graham-Smith 2005).

By addition of the amplitudes only of the harmonics, called incoherent addition, they can be combined such that the detectability of the signal is increased, allowing them to be distinguishable from noise. This method of addition can be repeated, generating a stronger signal without a significant effect on the noise, improving the signal-to-noise ratio for a narrow pulse over a sinusoidal one by the same factor as in the periodogram analysis (Lyne and Graham-Smith 2005). Often, searches must be carried out over different values of dispersion measure. Due to the propagation of the signal through the interstellar medium, there will be an observed delay of the signal due to interaction with ionized gas. The dispersion measure is a measure of the total electron content between the pulsar and observer and its value can effect the frequency and intensity of the signal. The search over the domain of dispersion measure is carried out much in the same way as the periodogram or Fourier analyses, using different

delays to coherently add signals from various receiver channels or performing a two-dimensional Fourier transform on the sample time versus receiver channel data and analyzing the spectrum (Lyne and Graham-Smith 2005).

These basic methods are made computationally relevant for long data sets with the use of folding algorithms and the fast Fourier transform (FFT). This is especially true for millisecond pulsars, which were not first discovered until the 1980's, when only a few were discovered by large-scale surveys. The majority of those discovered initially were found by searching specific objects of interest, or in areas where there was a good chance of finding them such as SNRs (Francis Graham-Smith 1992). This is because, for a given dispersion measure, the data processing necessary is determined by the inverse square of the minimum period searched. In particular, if the sampling rate is double to detect shorter period pulsations, then the number of frequency channels must also double, such that the dispersion broadening will remain the same fraction of the period (Lyne and Graham-Smith 2005). The increased number of millisecond pulsar discoveries since 1990 when inexpensive and more advanced computing power became available is clearly shown in the figure below.

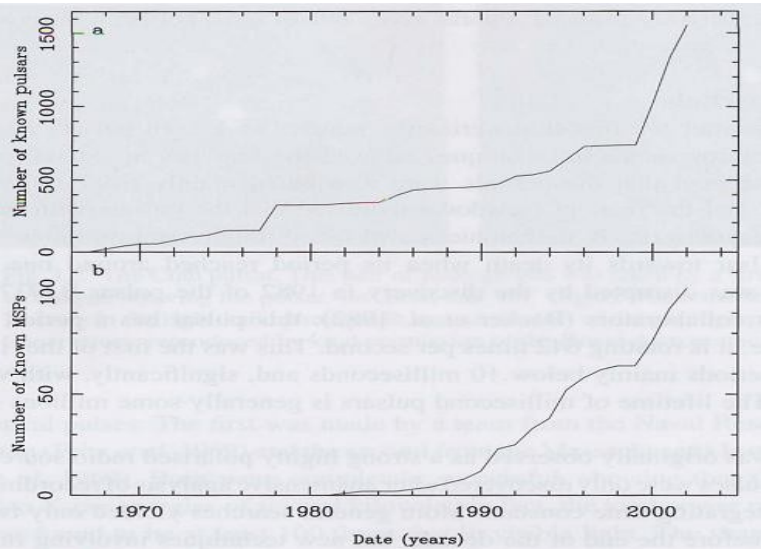


Figure 13: Time line depicting the number of a) all known pulsars and b) millisecond pulsars (Lyne and Graham-Smith 2005).

In addition to announcing the first pulsar discovery, Hewish's Nature paper of 1968 proposed a few details of the radio pulse easily gathered from its analysis. Apart from deducing that the source must be a rotating neutron star Hewish was able to show that the Doppler effect on the arriving time suggested the source lay outside the solar system and that the pulse arrival time depended on its frequency; a frequency dispersion effect resulting from interaction with electrons in the interstellar medium (Hewish et al. 1968). While pulsar surveys were initially conducted at or below 400 MHz, high frequencies were later used when low-noise receivers and larger bandwidths became available. The high frequencies lessened the effects of interstellar dispersion and scattering but had the effect of narrower beam widths, slowing the searches; however, this latter problem was avoided with the use of multiple beams, each with its own receiver (Lyne and Graham-Smith 2005). Radio pulse characteristics can be used to determine a precise localization of the pulsar. Since the Earth is rotating around the Sun the delay in pulse arrival time changes based upon where the various bodies are in orbit. The pulses from a pulsar in the plane of the ecliptic arrive earlier when the Earth is closer to the pulsar and later when it is further, with a six month difference from between maximum and minimum delay. A correction to pulse arrival data must also be made due to the motions of the Sun with respect to the center of inertia of the Solar System, known as the barycenter. This point moves relatively constantly through space and is used as an inertial reference frame (Lyne and Graham-Smith 2005). The propagation time of the signal from the barycenter to Earth is calculated using an ephemeris of the Earth's motion taken from planetary radar measurements (Manchester and Taylor 1977).

## 4.4 – Analysis Using Fermi Satellite

The combination of improvements implemented on the Fermi satellite combine to result in greater than a factor of 30 increase in sensitivity when compared to EGRET. This value is even higher at energies above 10 GeV. In addition, it will provide detailed analysis of the 10 – 100 GeV range, which is

largely unexplored (Thompson 2008). In short, the Fermi satellite has a myriad of improvements which will greatly further our knowledge of high-energy emission, and its sources, throughout the universe; however, its principal ability for discussion here will be its analysis of gamma-ray pulsars. While the LAT should be able to tell us a number of things concerning pulsars, such as the mechanisms driving their high-energy emission, as well as important population statistics, I will focus on its use in discovering new gamma-ray pulsars, principally those without radio counterparts. Previously, the intermittent nature of gamma-ray pulsar data has made their discovery difficult, especially without radio or X-ray timing information. However, Fermi will detect in the first two years of its scanning mode 25-30 times as many photons for most pulsars as did EGRET in its lifetime, suggesting "detections intrinsically 25 times fainter or 5 times farther away" (Thompson 2008). Although the LAT certainly has the necessary capabilities, estimates of the number of pulsar discoveries vary from tens to many hundreds of pulsars. The table below illustrates one such prediction for Fermi.

| | Normal pulsars | | Millisecond pulsars | |
|---|---|---|---|---|
| | Radio-loud | Radio-quiet | Radio-loud | Radio-quiet |
| Low Altitude Slot gap [10][27] | 81 | 43 | 16 | 99-131 |
| High Altitude Slot gap [13] | 5 | 49 | | |
| Outer Gap [13] | 1 | 258 | | |
| [17] | 78 | 740 | | |

Figure 14: Table listed predicted pulsar populations to be detected by Fermi (Harding 2007).

4.5 – Limiting Factors

In light of the many compelling facts to suggest the great abilities of the LAT to vastly increase the known gamma-ray pulsar population, there are many factors which make finding these objects difficult. It seems one of the main questions is not whether the LAT will detect photons from a great many new pulsars, but whether their pulsations will be identifiable in this photon data. These pulsations will be found by "1)'folding' of the events using timing ephemerides for known radio pulsars; 2) searches of

associated X-ray sources to find radio-quiet Geminga-like pulsars, or very faint radio pulsars or 3) 'blind' searches of the gamma-ray events" (Ransom 2007). The third method is that employed in this discussion, and will be reviewing in detail in subsequent sections. The factors limiting the detection of pulsations have largely to do with the emission properties of gamma-ray pulsars. One factor in particular is their low count rates of $10^{-7} – 10^{-8}$ photons $cm^{-2}$ $s^{-1}$ at energies greater than 100 MeV. This rate corresponds to 0.2 – 2 events per hour for the LAT, requiring observations over many weeks or even years to confirm a meaningful detection (Ransom 2007). Further difficulty is introduced by the high spin-down rates of young gamma-ray pulsars. Furthermore, these pulsars exhibit timing noise and, on month or year timescales, tend to "glitch" and change their observed frequency and frequency derivative. On observations taken over the timescales required to detect gamma-ray pulsations search methods must account for these changes and search over possible values of $f$ and $\dot{f}$ . It is also important to realize for example that if a viewing period is increased by a factor of ~3 to account for low photon fluxes due to a scanning mode of observation the probability that a detected signal with the same power as that from a shorter pointed observation is significant decreases by a factor of $\sim 3^3 = 27$ because of the large number of trials searched (Ransom 2007).

A particular problem with blind searches for gamma-ray pulsars is the uncertainty in position of the source. This error was estimated by Chandler et al. for a two week viewing period of EGRET data (2001). A Doppler shift, caused by the Earth's orbital motion, of the observed frequency in the barycenter corrected photon data is introduced. An error of ε in source location will result in an error of $\delta f$ in the frequency of

$$\delta f = v/c \; \varepsilon \sin \theta,$$

where θ is the angle between the earth's orbital velocity $v$ and the source direction (Chandler 2001). For relatively short viewing periods, this will not greatly affect the ability to detect pulsations, but the

determined frequency will be incorrect. The error in frequency derivative (or spin-down rate) is found by taking a derivative of the above equation to yield an error of

$$\delta \dot{f} = \frac{v}{c} \epsilon f \sin\theta .$$

Further differentiation leads to a second-order error of

$$\delta \ddot{f} = \dot{\theta}^2 \delta f + O(\dot{\theta})^3 .$$

In addition to making determination of the pulsation frequency difficult, these effects will cause the source frequency to drift over the course of the observation. This means the signal power in the FFT will be spread over many spectral bins. Furthermore, an inability to account for the second-order error in $\dot{f}$ will lead to a broadening of the signal peak (Ziegler 2008).

In the past, one of the major obstacles limiting the detection of pulsed emission from high-energy young and millisecond pulsars has been the required computational capabilities. Since the gamma-ray flux from these high-energy emitters is low in comparison to that at other wavelengths, data must be collected over many days, weeks, or even months. In addition to an observed effect from the pulsar spin-down making detection difficult, blindly searching long observation data sets requires an inordinate number of independent trials. For epoch folding searches, searching data sets over a range of $f$ and $\dot{f}$, the computational complexity is determined by $N \cdot T^2$, or $T^3$ for constant flux, where $T$ is the observation time and $N$ the number of photons. The use of the FFT is much more efficient, reducing the computational requirement to about $T^2 \cdot \log T$ (Ransom 2002 ASP). The required computer power is based upon the number of operations needed to perform, which is of order $N \cdot \log N$ for an FFT and of order $N^2$ for the discrete Fourier transform (DFT). Ransom gives, as an example, the case of a $10^6$ s observation, which requires a 10 gigapoint FFT for a full resolution analysis (Ransom 2002 ApJ). In order to reduce necessary computer power in searching for gamma-ray pulsars I adopted the

time-differencing method developed at the Santa Cruz Institute for Particle Physics (Atwood 2006).

4.6 – The Time-Differencing Method for Pulsar Blind Searches

A major tenet of the time-differencing method is to remove the smearing of the signal in the FFT power spectrum caused by phase slippage over the course of the observation. Atwood et al. developed their method based on the idea that a period signal in a series of timing data will also show up in the difference between pairs of photon arrival times (2006). Choosing time differences up to a certain maximum will reduce computational restrictions by diminishing the size of the FFT (Ziegler et al. 2008). I will outline the essence of the time-differencing method here; however, further details can be found in Atwood et al. (2006) and Ziegler et al. (2008). Gamma-ray pulsar searches must begin by correcting the barycentered photon arrival time data for the effects of the frequency derivative using

$$t_i = \tilde{t}_i + \frac{1}{2}\frac{\dot{f}}{f}\tilde{t}_i^2,$$

where $t_i$ are the corrected arrival times. Since we are conducting a blind search, and therefore have no information about $\dot{f}$ or $f$, the search must be conducted over steps in the ratio $\dot{f}/f$. The size of this step can be larger than in other methods because coherence must be maintained over a smaller timespan. The corrected arrival times are binned in $1/(2f_{\max})$ samples, where $f_{\max}$ is the maximum frequency being searched (Atwood 2006). Once normalized frequency amplitudes are calculated from the DFT, the power spectrum is searched for peaks from pulsar candidates (Ziegler 2008). For differences less than $T_{\text{MaxDiff}} = T_v/N_w$, a DFT is performed of the differences between photon arrival times:

$$D_l^{N_w} = \sum_{m=k+1}^{M} \sum_{k=0}^{N-1} a_k a_m \mathrm{e}^{-i2\pi l(m-k)/N}$$

where $a_k$ is the number of photons in the $k$th time sample, $N$ the number of time samples, $T_v$ the length

of the viewing period, and the upper limit of the outer summation is given by M = min (N – 1, $k$ + $N/N_w$).

A double loop is performed over the photon time bins, filling an array of size $2f_{\max}T_w$, summing the product $a_m a_k$ in the array's $m - k$ element, the result of which is then input into an FFT optimized for data having no imaginary component. For each photon, the time differences between it and all successive photons are included, out to a maximum of $T_w$. For gamma-ray photon data the count rates are low and this process is fast (Atwood 2006). To reduce the size of the DFT, the major goal of this method, it is to include only those difference windows that are short in comparison to the viewing period. In order to restrict the signal power from the entire viewing period into one frequency bin the error in the frequency derivative used to correct the data must obey

$$\delta \dot{f} < \frac{1}{T_w T_v} = \frac{N_w}{T_v^2}.$$

Due to leakage of power into the imaginary component of $D_l^{Nw}$ and other factors discussed in Atwood et al. (2006), the power in the periodicity search is defined as $|D_l|$ instead of the real part only, which is the traditional Fourier power in the case where the maximum difference window equals the total viewing period (Ziegler et al. 2008, Atwood et al. 2006). By maintaining coherence within a small window $T_{MaxDiff}$ of the full viewing period this method is able to significantly reduce CPU time, in comparison to the full FFT, without a great loss of sensitivity. It is achieves better sensitivity and a factor of $T_{MaxDiff}/T_v$ reduction in CPU time over the "stacking" method, which combines power spectra from subsequent time bins (Ziegler et al. 2008). These reasons make this blind search method ideal for detections of gamma-ray and millisecond pulsars, which require long data sets, with reasonable computer resources.

4.7 – Fermi Data Acquisition and Processing

The primary mode of observation for Fermi, especially during the first year, is called the "scanning" mode. This makes best use of the large field-of-view of the LAT by pointing the z-axis of the instrument 35º from the zenith in either direction in consecutive orbits. This allows for uniform sky exposure every 2 orbits, or about 3 hours for the Fermi orbit (Atwood et al. 2009). After track and energy reconstruction, gamma-ray events are analyzed to determine the accuracy of both of those determinations as well as whether or not they are in fact gamma-rays and not cosmic rays or other background particles. Once on board processing has completed data is downlinked in 1.5 GB sets every 2 orbits (3 hours) continuously and sent to the LAT Instrument Science Operations Center (ISOC). The data is further analyzed for energy and track resolution as well as the nature of the source, its direction, arrival time, and associated errors (Atwood et al. 2009).

For the purposes of gamma-ray pulsar searches, the data are further processed to gather a list of targets which have potential for being sources of interest. Source catalogs are populated based upon characteristics of the photon flux once particular fitting algorithms are applied to the Fermi data. Over the course of the scanning mode, as further data is gathered, the source list will grow and change as some become more significant, gaining more photons, or become less so, exhibiting more background. These catalog sources (areas of high photon density) can be analyzed with known locations to extract data from the general Fermi catalog, sometimes gaining better localization. Promising locations from both multiwavelength studies as well as a preliminary LAT source catalog are used to create a good candidate list. This list is further analyzed to pay special attention to sources in the Galactic plane, with a lack of longterm variability, and near a SNR or likely neutron star and remove those locations which may be associated with active galactic nuclei. This resulted in a list of about 200 locations, 36 of which were coincident with previously known EGRET locations (Abdo et al. 2009 "Detection of 16

Gamma-Ray Pulsars Through Blind Frequency Searches Using the Fermi LAT").

## 5 – Millisecond Pulsar Search Effort

As in Abdo et al. , I applied the time-differencing blind search technique to data gathered during the period beginning 4 August 2008 and ending 5 December 2008 (2009 "Detection of 16 Gamma-Ray Pulsars Through Blind Frequency Searches Using the Fermi LAT"). The data were barycenter corrected using the JPL DE405 Solar System ephemeris based upon the source position being either a candidate counterpart, found with multiwavelength observations, or a best estimate from LAT data. Cuts were made to accept "Diffuse" class photons falling within a 0.8º radius of the source location with energy over 300 MeV (Abdo et al. 2009 "Detection of 16 Gamma-Ray Pulsars Through Blind Frequency Searches Using the Fermi LAT", Atwood 2009). These choices best optimize the signal to noise ratio, background rejection of charged particles, and likelihood of finding pulsar photons, which tend to have higher energies.

The analyses I performed stemmed greatly from that described in Abdo et al. (2009 "Detection of 16 Gamma-Ray Pulsars Through Blind Frequency Searches Using the Fermi LAT"), making use of the time-differencing method developed by Atwood et al. (2006) and further applied to gamma-ray data by Ziegler et al. (2008). The difference was in searching especially for millisecond pulsars, which requires extending the frequency searched out to hundreds or thousands of hertz. Due to the fact that up to four harmonics are searched, detecting a frequency of 256 Hz would require a search out to 1024 Hz, or for a 512 Hz detection a search to 2048 Hz is required, and so on. This vast increase in frequency range requires either a large reduction in differencing window or a ramp up of computer power. The searches were designed to use the largest differencing window possible for the frequency

searched, without maxing out the computer power available. With access to a 32 GB processor on the UC-Santa Cruz campus, I was able to achieve the same differencing window discussed in Abdo et al. ($2^{19}$ s) for a search out to 512 Hz (2009 "Detection of 16 Gamma-Ray Pulsars Through Blind Frequency Searches Using the Fermi LAT"). For higher frequency searches the differencing window was necessarily reduced in powers of two, namely a search to 1024 Hz used a window of $2^{18}$ s and a search to 2048 Hz used a window of $2^{17}$ s. Higher frequency windows were not searched because the necessary reduction in differencing window was too great for proper detections to be made. Another consideration is the amount of time required for the search. When the process is performed at maximum memory utilization it takes about 7 minutes per source, which requires a few days when using lists of many hundreds of sources. The 200 locations discussed above can translate to source lists numbering 500 or more, often due to multiple locations or updates for a particular source adding duplicates.

In some cases, these searches to high frequencies produced results right away. The initial blind search I ran carried out to 512 Hz and was able to make detections of a number of the new gamma-ray pulsars being presented in Abdo et al. (2009 "Detection of 16 Gamma-Ray Pulsars Through Blind Frequency Searches Using the Fermi LAT"). This represented a significant test of the search method when performed over a larger frequency range. The initial searches were able to detect pulsations from pulsars J0007+7303, J0357+32, and J1741-2054 (Abdo et al. 2009 "Detection of 16 Gamma-Ray Pulsars Through Blind Frequency Searches Using the Fermi LAT"). Once I was able to determine the ability of the blind search method at higher frequencies and had performed trials to determine the best combinations of maximum frequency and differencing window for the available computer power I was able to focus on the goal of detecting millisecond pulsars.

I began by attempting to detect pulsations from a couple of known millisecond pulsars, J2124-3358 and J0030+0451. The first to show up was J0030+0451, as in Abdo et al. (2009 "Discovery of a Population of Gamma-Ray Millisecond Pulsars with the *Fermi* Large Area Telescope" and "Pulsed Gamma-rays from the millisecond pulsar J0030+0451 with the Fermi Large Area Telescope"), found at a frequency of 205.53 during a blind search using a maximum frequency of 1024 Hz and a differencing window of 218 seconds. Then, the pulse signal was refined using an epoch-folding search over a small region of frequency and frequency derivative, the resulting light curve is shown in Figure 15 below (Abdo et al. 2009 "Detection of 16 Gamma-Ray Pulsars Through Blind Frequency Searches Using the Fermi LAT"). This refinement uses the frequency and frequency derivative values found in the blind search to make a finer search over smaller windows around the given values, generally leading to a better signal detection. The same analysis was performed for PSR J2124-3358 without a significant initial detection. The source parameters were refined and by searching a smaller frequency window around the known frequency a frequency of 202.79 Hz resulted. The power spectrum is shown in Figure 15 below. This analysis is obviously ineffective as a blind search; however, is a useful method for detection of gamma-ray pulsations from known radio or X-ray counterparts.

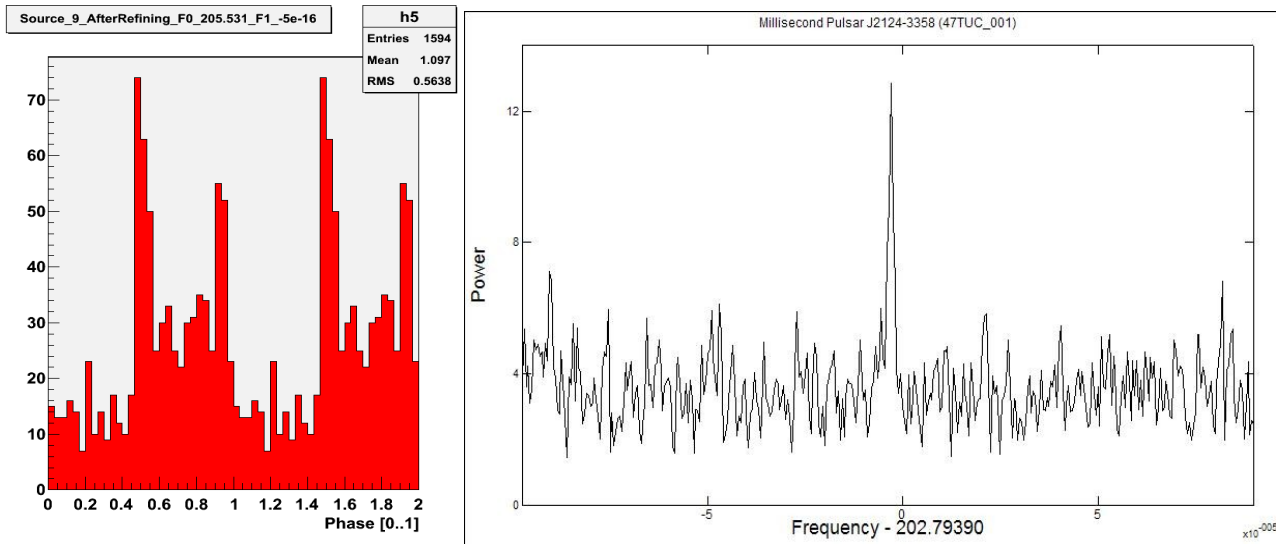


Figure 15: On the left is the refined light curve for PSR J0030+0451 and the right is the power spectrum for PSR J2124-3358.

Upon confirmation of the ability of the time-differencing method to detect higher frequency pulsations I set out to attempt to find a new, or unknown, millisecond pulsar. First, it was necessary to refine the LAT source list to those that were more likely to be millisecond pulsars. Sources were removed with known associations, be they pulsars, blazars, or AGNs. Then, since most MSPs are found at higher latitude, those locations with a galactic latitude B of greater than 5 degrees were selected. This is due to a higher average lifespan allowing for significant drift from the Galactic plane as well as preferential detection of those close to the Solar System. This, however, still meant a list of 178 sources. Upon running multiple blind searches at the aforementioned frequency and differencing window trials I was able to create a shortened list with those sources producing the highest number of photons. Those candidate sources were analyzed and refined, but no significant new detection resulted.

5.1 – Errors and Improvements

There are a number of factors which make the detection of millisecond pulsars especially difficult. Many of these are compounded when searching gamma-ray data alone. Since half of all millisecond pulsars lie in binary systems, the lack of knowledge of the orbital characteristics of the system when performing a blind search make resolving pulsations nearly impossible. In the rare case that the plane of the binary orbit is pointing directly at Earth detections are possible, but still difficult. Furthermore, low gamma-ray photon counts are typical of millisecond pulsars, requiring viewing periods extending over many months. In that case the effect on frequency error due to positional uncertainty is even greater than that estimated in Chandler et al. (2001). At the start of the observation, the frequency is only off by about $v/c \cdot \varepsilon^2 \cdot f$, for a velocity $v$, frequency $f$, and positional error of $\varepsilon$. For small values of $\varepsilon$ this effect is not enough to prevent detection. However, three months later the frequency is now off by about $v/c \cdot \varepsilon \cdot f$, causing a spread of the photons in the power spectrum. With searches using a large number of bins, it is likely there will be many bins in the spectrum in that frequency range, making the

detection impossible. In effect, the 2nd-order effect discussed in Chandler becomes just as significant as the 1st-order effect, resulting in a peak that is not only shifted in frequency, but also spread out by the same amount. This effect is even greater for the 4 month long observation I performed, and for the 6 month observation most likely necessary to detect a millisecond pulsar the effect is twice as large. If the frequency spread is not to exceed $1 \cdot 10^{-4}$, then the positional uncertainty would have to be less than 0.25º. Again, a 6-month observation would require twice as much refinement, at this point only possible with data from other wavelengths, making blind gamma-ray detections of millisecond pulsars extremely difficult.

## 6 – Conclusion

Pulsar astronomy has changed significantly since the discovery of the first pulsar over forty years ago. It is clear that pulsars are rapidly rotating highly magnetized neutron stars and their creation and evolution is largely understood. Improvements in telescope technology beginning with fast receiving radio antennae, to probes of higher energy radiation, to the present space based gamma-ray satellites like the Fermi Gamma-Ray Space Telescope have lead to the discovery of a large number of pulsars, allowing for greater understanding of their emission mechanisms. This new wave of technology has allowed for the discovery of many new gamma-ray pulsars through blind search methods. The recently developed time-differencing technique has much improved the sensitivity of such searches with reasonable computational demands and has proved effective in its use on Fermi gamma-ray data. A probe into the possibility for the discovery of new millisecond pulsars, a class of high frequency pulsars, has been made which tests the limits of current telescope capabilities. Continued observation and data collection could yield results; however, the prospect for discovery of new radio quiet millisecond pulsars will rely much on improved telescope sensitivity in the future.

Works Cited

Abdo, A.A., *et al.* (2009) ApJ, submitted – "Pulsed Gamma-rays from the millisecond pulsar J0030+0451 with the Fermi Large Area Telescope."

Abdo, A.A., *et al*. (2009) Science, submitted – "Detection of 16 Gamma-Ray Pulsars Through Blind Frequency Search Using the Fermi LAT."

Abdo, A.A., *et al*. (2009) Science, submitted – "Discovery of a Population of Gamma-Ray Millisecond Pulsars with the *Fermi* Large Area Telescope."

ATNF Pulsar Catalog (May 2009) http://www.atnf.csiro.au/research/pulsar/psrcat/.

Atwood, W.B., Ziegler, M., Johnson, R.P., & Baughman, B.M. (2006) ApJ, **652:** L49-L52.

Atwood, W.B. *et al*. (2009) ApJ, **697:** 1071-1102.

Baade, W. & Zwicky, F. (1934) Proc. Nat. Acad. Sci., **20:** 259-263.

Backer, D.C., *et al.* (1982) Nature, **300:** 615-618.

Bhattacharya, D. & van den Heuvel, E.P.J. (1991) Physics Reports, **203:** 1-124.

Chiang, J. & Romani, R. (1992) ApJ, **400:** 629.

Chandler, A.M., *et al*. (2001) ApJ, **556:** 59-69.

European Space Agency (May 2009) "About INTEGRAL," http://www.sciops.esa.int/index.php?project=INTEGRAL&page=index

Goddard Space Flight Center (May 2009) "Compton Gamma-Ray Observatory (CGRO)," http://heasarc.gsfc.nasa.gov/docs/cgro/cgro.html.

Graham-Smith, F. (1992) *Contemporary Physics*, 33: 165-173.

Harding, A.K. (2007) "Pulsar Physics and GLAST," in *Proc. of First GLAST Symposium*, edited by S.Ritz, P.F. Michelson, and C. Meegan, AIP Conf. Proc. **921:** 49-53.

Hartman, D.L., *et al.* (1999) ApJ Supp. Ser., **123:** 79-202.

Heuvel, E.P.J. van den. (1987) "Millisecond Pulsar Formation and Evolution," in *The Origin and*

*Evolution of Neutron Stars*, edited by D.J. Helfand and J.-H. Huang, IAU Ser. **125:** 393-406.

Hewish, *et al.* (1968) Nature, **217:** 709.

Longair, M.S. (1994) *High Energy Astrophysics: Second Edition* (Cambridge: Cambridge University Press)

Lyne, A.G. & Graham-Smith, F. (2005) *Pulsar Astronomy: Third Edition* (Cambridge: Cambridge University Press).

Manchester, R.N., Hobbs, G.B., Teoh, A., & Hobbs, M. (2005) AJ, **129:** 1993-1006.

Manchester, R.N. & Taylor, J.H. (1977) *Pulsars* (San Francisco: W.H. Freeman and Company).

Pacini, F. (1967) Nature, **216:** 567.

Possenti, A. & Burgay, M. (2008) "Millisecond radio pulsars and their relatives," in *Decade of Accreting Millisecond X-ray Pulsars, Proceedings of the International Workshop* edited by R. Wijnands, D. Altamirano, P. Soleri, N. Degenaar, N. Rea, P. Casella, A. Patruno, and M. Linares, AIP Conf. Proc. **1068:** 117-124.

Ransom S.M. (2002) "Fast Search Techniques for High Energy Pulsars," in *Neutron Stars in Supernova Remnants*, edited by P.O. Slane & B.M. Gaensler, ASP Conf. Ser. **271:** 361-364.

Ransom, S.M. (2007) "Finding (or not) New Gamma-Ray Pulsars with GLAST," in *Proc. of First GLAST Symposium*, edited by S.Ritz, P.F. Michelson, and C.Meegan, AIP Conf. Proc. **921:** 54-56.

Ransom, S.M., Eikenberry, S.S., & Middleditch, J. (2002) ApJ, **124:** 1788-1809.

Smith, D.A., *et al*. (2008) A&A, **492:** 923-931.

Thompson, D.J. (2008) "Gamma-Ray Pulsar Studies with GLAST," in *40 Years of Pulsars – Millisecond Pulsars, Magnetars, and More*, edited by C.G. Bassa, Z. Wang, A. Cumming, & V.M. Kaspi, AIP Conf. Proc. **983:** 56-63.

Ziegler, M., Baughman, B.M., Johnson, R.P., & Atwood, W.B. (2008) ApJ, 680: 620-626.